metals

MDPI

Communication

Effects of Sc and Be Microalloying Elements on Mechanical Properties of Al-Zn-Mg-Cu (Al7xxx) Alloy

Sung-Jae Won [1,2], Hyeongsub So [1,2], Jung-Woo Han [1,2], Soong Ju Oh [2], Leeseung Kang [1] and Kyou-Hyun Kim [1,*]

[1] Korea-Russia Innovation Center, Korea Institute of Industrial Technology, Incheon 21655, Republic of Korea
[2] Department of Materials Science and Engineering, Korea University, Seoul 02841, Republic of Korea
* Correspondence: khkim1308@kitech.re.kr; Tel.: +82-32-226-1360

Abstract: We demonstrate via comprehensive microstructural investigation the effects of Sc and Be microalloying on the mechanical properties of Al-Zn-Mg-Cu-based alloys, where Sc microalloying enhances the tensile properties of an Al-9.0Zn-3.0Mg-3.0Cu alloy from 645 MPa (ε_f = ~6%) to 672 MPa (ε_f = ~8%). In contrast, simultaneous microalloying with Sc and Be reduces the mechanical strength of a synthesized Al alloy to 654 MPa (ε_f = ~8%). Comprehensive microstructural investigation revealed that Sc microalloying leads to Al grain refinement, the formation of hardening ($MgZn_2$, Al_3M) phases, and an increase in the solid solution of Al. Additional Be microalloying also enhances the formation of $MgZn_2$ phase, while Al_3M (M: Zr, Sc) type phases are restrained from forming in Al grains. Furthermore, solid solution in Al grains is reduced by the trace addition of Be microalloying, resulting in an increase in large intermetallic compounds at Al grain boundaries.

Keywords: 7xxx series aluminum alloy; mechanical properties; microalloying

Citation: Won, S.-J.; So, H.; Han, J.-W.; Oh, S.J.; Kang, L.; Kim, K.-H. Effects of Sc and Be Microalloying Elements on Mechanical Properties of Al-Zn-Mg-Cu (Al7xxx) Alloy. *Metals* **2023**, *13*, 340. https://doi.org/10.3390/met13020340

Academic Editor: Lihua Zhan

Received: 9 January 2023
Revised: 31 January 2023
Accepted: 6 February 2023
Published: 8 February 2023

1. Introduction

Thermomechanical processing is conventionally used to optimize the mechanical properties of heat-treatable Al alloys [1,2]. The main purpose of thermomechanical processing is to induce microstructural evolution in as-cast Al alloys so as to yield proper mechanical properties. As well as thermomechanical processing, the addition of trace amounts of alloying elements, a process known as microalloying, is often applied to achieve optimized combinations of mechanical properties in Al alloys [3–6]. Like thermomechanical processing, microalloying directly affects the nature of Al alloys, such as their morphology, chemistry, spatial distribution, and size of precipitates [7–10]. Additionally, microalloying helps the thermomechanical process promote microstructural evolution for the clustering and precipitation processes. This then results in grain refinement or increased hardening precipitation [11,12]. Thus, the combination of thermomechanical processing and the microalloying technique is an effective way to enhance the performance of Al alloys.

Among the reported microalloying elements, Sc microalloying has been widely investigated to optimize the mechanical properties of Al alloys. Fine Al_3M-type ($L1_2$ ordered structure, FCC) precipitates are generally observed in Al grains when trace amounts of Sc are added [13–16]. The Al_3M-type phase is known to precipitate during the solidification step [17,18]. This then generates heterogeneous nucleation sites for Al, leading to refinement of the Al grain. In addition, the formation of Al_3M-type precipitates improves the mechanical properties by hindering dislocation motion, the migration of subgrain boundaries, and nucleation and grain recrystallization [19,20]. Furthermore, Al_3M-type precipitates have been reported to provide additional nucleation sites for metastable η′ and equilibrium η phases [21–27].

In addition to the microalloying element Sc, the light metal Be has been also used as a microalloying element to optimize the mechanical properties of Al alloys [28,29]. In one previous report, Be microalloying was revealed to facilitate extensive dislocation loop

structures during the aging process [30]. The dislocation loop structures then provide additional sites for heterogeneous nucleation of the precipitation hardening phase in the Al matrix [31]. Moreover, Al forms no intermetallic compounds with Be, thus inhibiting the formation of large particles at the grain boundaries, which act as crack initiation sites [32].

Recently, multi-strengthening mechanisms have been investigated in a modified Al7056 alloy with the microalloying element of Sc [33]. The mechanical strength of the reported alloy was greatly improved by accelerating the formation of hardening precipitates via an increase in the Zn:Cu:Mg (3:1:1) ratio. Next, trace addition of Sc further enhanced the tensile strength of the reported Al alloy by refining the Al grain. According to the previous work, trace addition of Sc induces the formation of Al_3Sc, which acts as a heterogenous nucleation core for α-Al. As a result, the grain size of Al is severely reduced by approximately ~50% compared to the case of an alloy without Sc microalloying, leading to an increase in tensile strength of ~6%. Nevertheless, large particles formed at the grain boundaries act as crack propagation sites, so the reported Al alloy has a certain limitation in improving ductility [34,35].

Considering the above, trace addition of both Sc and Be microalloying elements can give rise to a potential method to enhance the mechanical properties of Al-Zn-Mg-Cu alloys by refining the Al grain, promoting the formation of hardening precipitates, and reducing large intermetallic particles formed at grain boundaries. We thus investigated the simultaneous effects of Sc and Be microalloying on the mechanical properties of a modified Al7056 alloy, which has not been carefully considered in previous studies. In this study, an Al-9.0Zn-3.0Mg-3.0Cu alloy was synthesized with trace additions of Sc and Sc + Be for comparison. Our observations indicate that Sc microalloying simultaneously affects the formation of hardening precipitates and grain refinement. Simultaneous microalloying effects of Sc and Be were demonstrated based on microstructural investigations from microscopic to nanoscopic scale. It was revealed that trace addition of Be impedes the formation of Al_3M phase, in a process that provides heterogeneous nucleation sites in the Al alloy. Herein, based on a combination of analytic methods, we discuss the effects of Sc and Be microalloying on the mechanical properties of an Al-Zn-Mg-Cu-based alloy.

2. Experimental Procedures

The nominal chemical compositions of the investigated alloys are given in Table 1. Hereinafter, the Sc/Be-free, Sc-added, and (Sc + Be)-added Al alloys will be respectively referred to as Al7, Al7Sc, and Al7SB. The developed Al alloys were initially prepared from Al (99.99%), Zn (99.99%), Mg (99.99%), and Cu (99.99%); the master alloys were prepared from Al-2wt.%Sc, Al-14wt.%Zr, and Cu-2wt.%Be. The prepared elements were then melted at 780 °C, and this temperature was maintained for 40 min with Ar degassing to ensure that Al_3M particles in the Al-2wt.%Sc and Al-14wt.%Zr master alloys completely melted. The molten metal was finally cast into molds (SKD 61) to produce as-cast Al alloys. Table 2 gives the chemical compositions of the as-cast Al7, Al7Sc, and Al7SB alloys as obtained by optical emission spectrometry (OES, Thermo Fisher Scientific Inc., ARL iSpark Series Optical Emission Spectrometer, Waltham, MA, USA). The as-cast samples were processed by homogenization treatment (470 °C/24 h) → hot rolling (reduction ratio: 70%) → solution treatment (470 °C/2 h, water quenching) → artificial aging. For the artificial aging, we used an aging temperature of 120 °C, which was used in a previous study [33]. Furthermore, we measured the hardness values of the synthesized Al alloys with respect to the hardening times; however, details of the experimental results are not provided in this study. For this study, in consequence, artificial aging was carried out to meet T6 temper (peak aging). Tensile testing was then carried out using a UTM (SHIMADZU, Universal Testing Machine, AG-300kNX plus) according to the ASTM E8/E8m-16a standard (standard test method for tension testing of metallic materials) with a strain rate of 1 mm/min.

Table 1. Nominal compositions of designed alloys.

Alloys	Chemical Composition (wt.%)						
	Al	**Zn**	**Mg**	**Cu**	**Sc**	**Be**	**Zr**
Al7	Bal.	9.0	3.0	3.0	-	-	0.08
Al7Sc	Bal.	9.0	3.0	3.0	0.1	-	0.08
Al7SB	Bal.	9.0	3.0	3.0	0.1	0.06	0.08

Table 2. As-cast nominal composition of designed alloys.

Alloys	Chemical Composition (wt.%)						
	Al	**Zn**	**Mg**	**Cu**	**Sc**	**Be**	**Zr**
Al7	Bal.	9.02	2.96	3.08	-	-	0.09
Al7Sc	Bal.	8.88	3.01	3.10	0.09	-	0.09
Al7SB	Bal.	9.06	2.93	3.06	0.08	0.04	0.08

The microstructure of the thermomechanically processed samples was investigated from the microscopic scale (~μm) to the nanoscopic scale (~nm). For microscopic scale microstructural investigation, we used optical microscopy (OM), secondary electron microscopy (SEM), and X-ray diffraction (XRD). For nanoscopic scale, details of the crystal structure were investigated using transmission electron microscopy (TEM). Specimens for TEM observation were prepared by mechanical polishing to obtain a sample thickness of <20 μm. The polished samples were then Ar-ion milled at an incident angle of 6° and an accelerating voltage of 3.5 kV for electron transparency (GATAN Inc., PIPS^{TM}, Precision Ion Polishing System, Pleasanton, CA, USA).

3. Results

Figure 1 shows the tensile properties of the T6-tempered Al7, Al7Sc, and Al7SB alloys. To obtain average values, we carried out tensile tests for each specimen more than ten times. As shown in Figure 1, the Al-9.0Zn-3.0Mg-3.0Cu alloy showed a tensile strength of 645 MPa (σ_{UTS}) with elongation of ~6.4%. Trace Sc addition improved the mechanical properties of the Al7Sc alloy to 672 MPa (σ_{UTS}), with elongation of 8.6% [33]. The tensile properties of the Al7SB alloy were also measured and found to be 625 MPa (σ_y) and 654 MPa (σ_{UTS}), with fracture strain of 8.2%. It was therefore determined that microalloying with both Sc alone and Sc + Be improved the tensile properties of the initial composition of Al-9.0Zn-3.0Mg-3.0Cu. Compared to the results for the Al7Sc alloy, however, the experimental tensile test results for Al7SB indicate that the tensile strength decreased with simultaneous addition of Sc and Be (672 MPa → 654 MPa), while the ε_f value showed no significant difference (8.6% → 8.2%).

Figure 2 shows typical optical micrographs (OMs) recorded from the Al7, Al7Sc, and Al7SB alloys. In the recorded OM image (Figure 2b), the Al grain size of Al7 can be seen to have been greatly reduced from ~222 μm to ~105 μm due to the trace addition of Sc. On the other hand, no reduction in grain size can be observed in the Al7SB alloy compared to that in the Al7Sc alloy. The average grain size of Al is ~108 μm, which is almost identical to that of Al7Sc. Nevertheless, the tensile strength of the Al7SB (654 MPa) alloy is lower than that of Al7Sc (672 MPa), as shown in Figure 1.

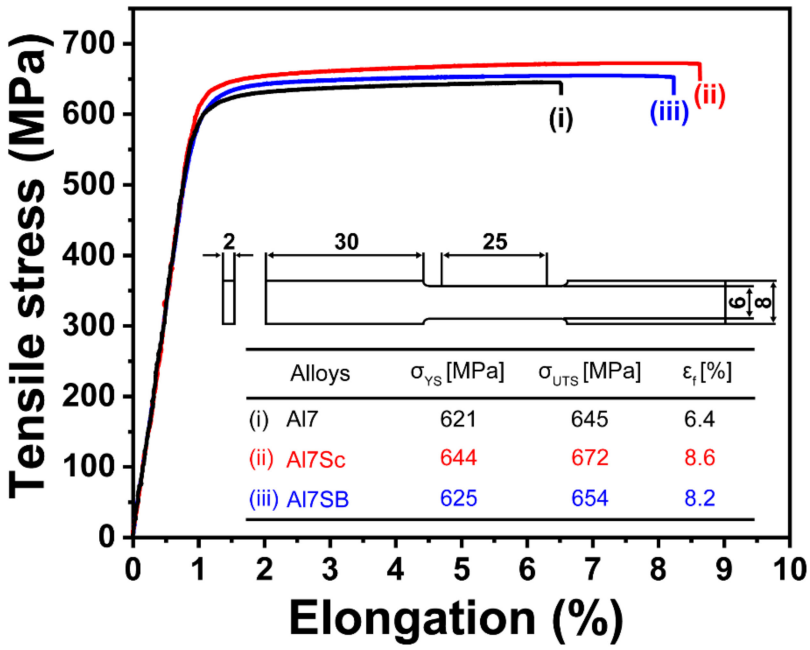

Figure 1. Experimental tensile tests performed on Al7, Al7Sc, and Al7SB alloys.

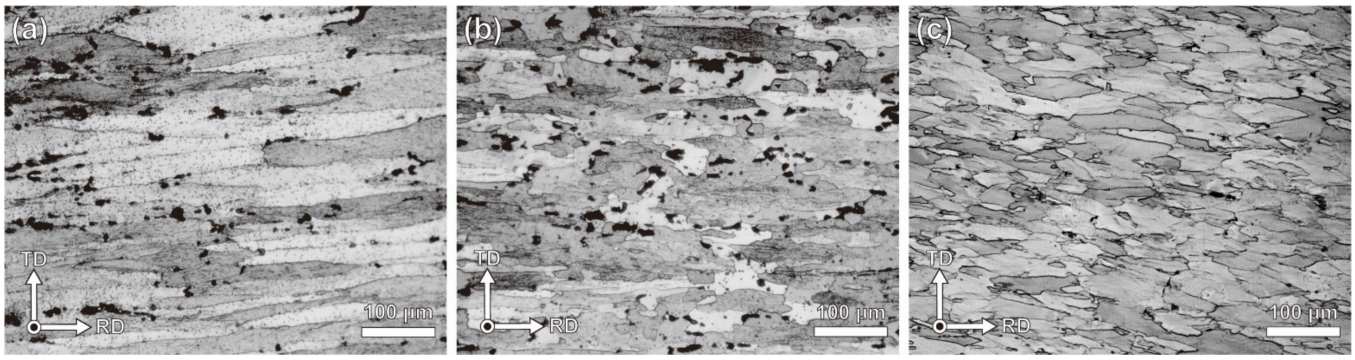

Figure 2. Representative optical microscope images recorded from T6-tempered (**a**) Al7, (**b**) Al7Sc, and (**c**) Al7SB. The rolling direction is indicated in the left corner of each OM image with TD (transverse direction) or RD (rolling direction).

Figure 3 shows the 2θ XRD profiles obtained from the Al7, Al7Sc, and Al7SB alloys. The recorded XRD profiles of the investigated alloys have exactly the same sets of strong and weak peaks. The indexing results indicated that the set of strong (major) peaks is the α-Al (FCC, $Fm\bar{3}m$) phase. Next, one of the other small peaks was indexed as $MgZn_2$ (HCP, $P6_3/mmc$). This phase is well known as the major strengthening phase in the Al-Zn-Mg-Cu alloy system. The remaining small peaks were then respectively identified as Al_2CuMg (S phase, Cmcm) [30,36] and $Mg_{32}(Al, Zn)_{49}$ (T phase, $Im\bar{3}$) [37,38], which are preferentially formed at grain boundaries of the Al 7xxx alloy system [39].

Figure 4a–c show representative back-scattered electron (BSE) images recorded from the Al7, Al7Sc, and Al7SB alloys. As can be seen in Figure 4a, the Al7 alloy consists of large intermetallic compounds at the grain boundaries of Al. Based on the XRD results, the large particles formed at the grain boundaries can be identified as S and T phases. These intermetallic compounds decreased in the Al7Sc alloy, so the overall microstructure of Al7Sc became more uniform compared to that of Al7. In contrast, the simultaneous additions of Sc and Be induced the formation of more intermetallic compounds at the grain boundaries of Al (Figure 4c). In consequence, considering the fraction changes of the S and T phases, it can be reasonably determined that Sc enhances the solutionization, while Be impedes it. On the other hand, trace additions of Sc and Be showed no evidence of

forming any Sc/Be-related phases at the macroscopic scale. This is because such Sc-related precipitates as Al_3M-type phase are only a few nanometers in size [40]. Details of the microstructural differences in the Al7, Al7Sc, and Al7SB alloys, therefore, will be discussed based on nanoscopic structural investigations using TEM.

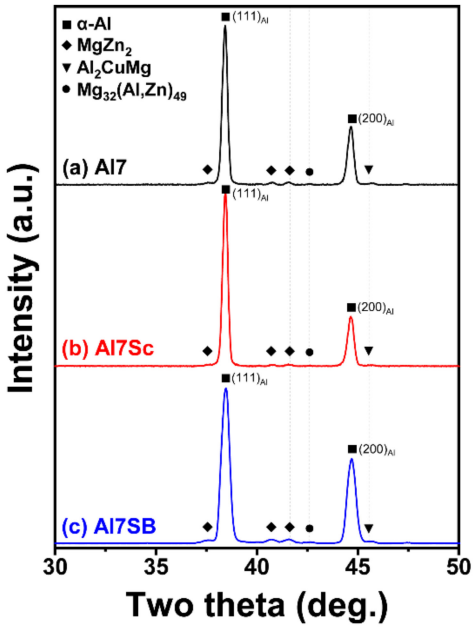

Figure 3. XRD profiles recorded from (**a**) Al7, (**b**) Al7Sc, and (**c**) Al7SB alloys.

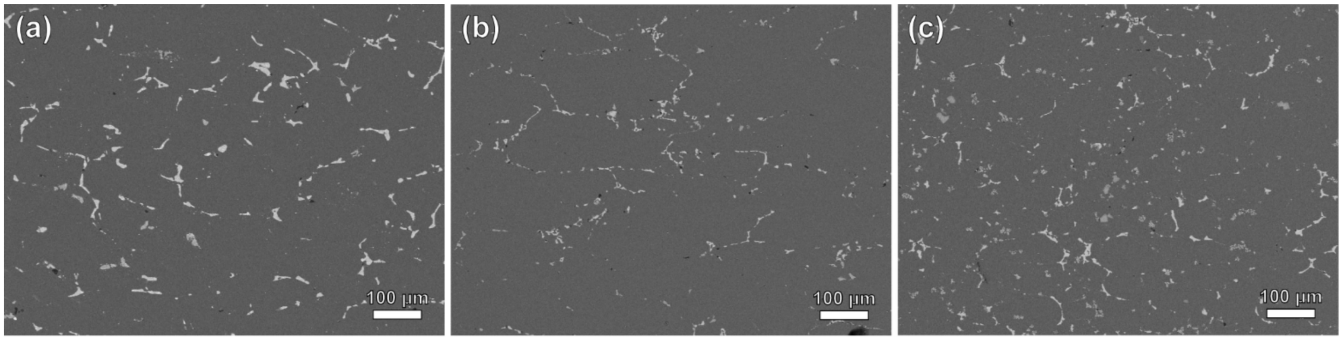

Figure 4. Back-scattered electron (BSE) images recorded from (**a**) Al7, (**b**) Al7Sc, and (**c**) Al7SB alloys.

Figure 5 provides typical bright field (BF) images and corresponding electron diffraction (ED) patterns of the Al7, Al7Sc, and Al7SB alloys, recorded at the zone axis of [110]Al. All TEM results were investigated along the zone axis of [110]Al, which is the best direction to observe precipitations formed in the Al grain. Two main types of precipitates can be found in the Al grain of the Al7 alloy, as shown in Figure 5a. The first are spherical precipitates (indicated by the arrow in Figure 5a), which have average diameters of 20.4 nm. These precipitates were identified as the Al_3Zr phase. The second are very fine precipitates observed in the dotted square (I) (Figure 5a), which have an average size of ~nm. These very fine nanoparticles were revealed as the $MgZn_2$ phase, known as the major hardening precipitate in Al7xxx series alloys. As shown in Figure 5b, the corresponding ED (electron diffraction) pattern has very weak streaks parallel to the {111} of the Al matrix. This indicates that the very fine $MgZn_2$ precipitates are formed along the {111} of the Al matrix. In addition, the strong diffraction spot at $\frac{1}{2}g_{\{200\}_{Al}}$ is the result of the Al_3Zr phase, as shown in Figure 5a. Details of the ED indexing can be compared to the calculated ED pattern shown in Figure 5c. The trace addition of Sc directly affects the formation of precipitates. As shown in Figure 5d, the $MgZn_2$ phase became larger than that of the Al7 alloy. The average size

of $MgZn_2$ was measured to be ~7.3 nm in length and ~2.8 nm in width. Interestingly, the diameter of the hardening precipitate ($MgZn_2$) was constant at ~2 nm for all investigated Al alloys. The number of hardening precipitates was manually counted from at least 10 phase contrast images. Furthermore, the relatively large precipitate of Al_3Zr disappeared in the Al grain of the Al7Sc alloy. Instead, Al_3Sc precipitates formed in the Al matrix, as shown in the inset of Figure 5d. Accordingly, as shown in Figure 5e, the ED pattern of Al7Sc shows that the intensity of streaks along the $\{111\}_{Al}$ is stronger than that of the streaks of the Al7 ED pattern due to the growth of $MgZn_2$ precipitates. Thus, the $MgZn_2$ precipitates in the Al7Sc alloy makes this alloy relatively stronger, which is rarely observed in the ED pattern of the Al7 alloy. As shown in Figure 5g, additional Be microalloying enhanced the growth of $MgZn_2$ precipitates in the Al7SB alloy. The average $MgZn_2$ precipitates were estimated to be between 10 and 15 nm in length, considerably larger than the average precipitate sizes in the Al7Sc alloy. The growth of $MgZn_2$ leads to strong diffraction, as shown in Figure 5h. Furthermore, due to the growth of $MgZn_2$ precipitate, streaks of $MgZn_2$ reflections became shorter than those in the ED pattern of Al7Sc alloy. On the other hand, the ED pattern of Al7SB showed no evidence of formation of any Al_3M-type phase.

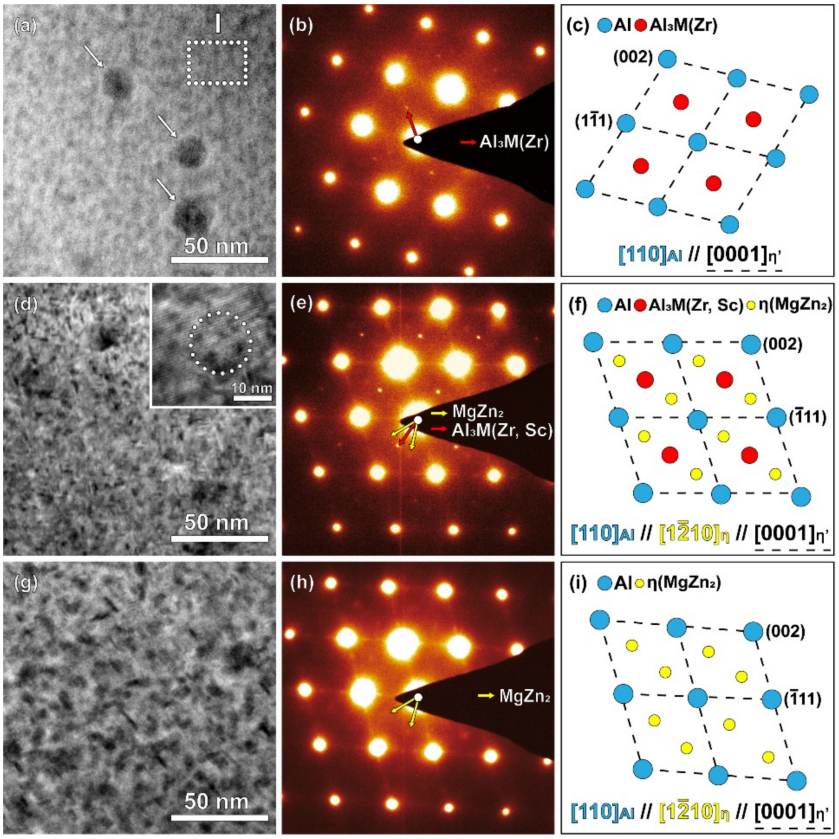

Figure 5. Typical bright field images and corresponding ED patterns of (**a**–**c**) Al7, (**d**–**f**) Al7Sc, and (**g**–**i**) Al7SB alloys. Details of ED indexing can be found in (**c**,**f**,**i**) calculated ED patterns.

4. Discussion

Comprehensive microstructural investigation was used to reveal the origin of the mechanical properties of Al7, Al7Sc, and Al7SB alloys. At the macroscopic level, the Al7 alloy has an average Al grain size of ~222 μm. The grain size of Al then significantly decreases in the Al7Sc and Al7SB alloys. The two alloys Al7Sc and Al7SB have similar Al grain sizes of 105~108 μm, with intermetallic compounds at the grain boundaries. Sc is well known to form Al_3Sc in the early stage of solidification, providing the formation of heterogeneous nucleation sites for Al [26,41]. This then results in the refinement of Al grain size. Thus, the grain refinement of Al7 alloy is affected only by the Sc microalloying element.

On the other hand, the volume fraction of intermetallic compounds decreases in the Al7Sc alloy. This thus suggests that the solubility of minor elements (Zn, Mg, and Cu) increases with trace additions of Sc in the Al7 alloy. This may result in the enhanced formation of $MgZn_2$ precipitates in the Al7Sc alloy. As shown in Figure 5, the major hardening precipitates of $MgZn_2$ are stimulated to grow by Sc addition, while the formation of relatively large precipitates (Al_3Zr) is restricted.

In contrast, additional Be microalloying increases the volume fraction of intermetallic compounds at the grain boundaries of Al. This then results in a decrease in solute elements in the Al grain of Al7SB. Nevertheless, the formation of $MgZn_2$ was enhanced compared to that of Al7Sc. Similarly, previous studies reported that relatively high amounts of Be (>0.07wt.%) rapidly accelerated the precipitation processes in several age-hardenable Al alloys [30], while the exact role of Be still remains subject to debate [42–44]. On the other hand, the addition of Be microalloying prevented the formation of such Al_3M-type phases as Al_3Sc and Al_3Zr in the Al7SB alloy. This, in consequence, resulted in a decrease in the number density of hardening precipitates in the Al matrix, lowering the mechanical strength of the Al7SB alloy [37,45].

5. Conclusions

In this study, we investigated the effects of addition of trace amounts of Sc and Sc + Be on the mechanical properties of Al-Zn-Mg-Cu-based (7xxx) alloys. Based on the macroscopic to nanoscopic scale structural investigations, microalloying of Sc alone and Sc + Be can be closely correlated with microstructural change, which is a key to change the mechanical properties of the studied Al alloys.

(1) Sc microalloying effect

Small addition of Sc induces grain refinement at the macroscopic scale regardless of Be microalloying. Al grain refinement was observed in both Al7Sc and Al7SB alloys. In addition, Sc helped improve the solid solution of minor elements in the Al grain. The relatively large intermetallic particles formed in the Al grain boundaries decreased in the Al7Sc alloy. At the nanoscopic scale, the formation of major hardening precipitates ($MgZn_2$) was facilitated by the Sc microalloying. These microstructural evolutions then resulted in improvement of the mechanical properties.

(2) Be microalloying effect

Additional Be microalloying led to different microstructural changes in the Al7 alloy. Al grain refinement was still observed in the Al7SB alloy due to the addition of Sc. The large intermetallic particles, however, increased in the Be-added Al7Sc alloy. Nevertheless, the addition of Be microalloying enhanced the precipitation formation of $MgZn_2$ phase while preventing the formation of such Al_3M-type phases as Al_3Sc and Al_3Zr in the Al7SB alloy. This, in consequence, lowered the mechanical properties of the Al7SB alloy compared to those of the Al7Sc alloy.

Author Contributions: Data curation, S.-J.W. and H.S.; funding acquisition, K.-H.K.; investigation, S.-J.W., H.S., J.-W.H. and L.K.; project administration, K.-H.K.; resources, S.J.O. and K.-H.K.; software, L.K.; supervision, S.J.O.; writing—original draft, S.-J.W.; writing—review and editing, K.-H.K. All authors have read and agreed to the published version of the manuscript.

Funding: This research was financially supported by the Institute of Civil Military Technology Cooperation, funded by the Defense Acquisition Program Administration and the Ministry of Trade, Industry and Energy of the Korean Government, under grant No. UM21308RD3. This study was also partially supported by the R&D program and research facilities of the Korea Institute of Industrial Technology.

Institutional Review Board Statement: Not applicable.

Informed Consent Statement: Not applicable.

Data Availability Statement: The raw/processed data required to reproduce these findings cannot be shared at this time as the data also form part of an ongoing study.

Conflicts of Interest: The authors declare no conflict of interest.

References

1. Wei, S.; Wang, R.; Zhang, H.; Xu, C.; Wu, Y.; Feng, Y. Influence of Cu/Mg ratio on microstructure and mechanical properties of Al–Zn–Mg–Cu alloys. *J. Mater. Sci.* **2021**, *56*, 3472–3487. [CrossRef]
2. Chen, Z.; Zheng, Z. Microstructural evolution and ageing behaviour of the low Cu: Mg ratio Al–Cu–Mg alloys containing scandium and lithium. *Scr. Mater.* **2004**, *50*, 1067–1071. [CrossRef]
3. Zuo, J.; Hou, L.; Shu, X.; Peng, W.; Yin, A.; Zhang, J. Grain refinement assisted by deformation enhanced precipitates through thermomechanical treatment of AA7055 Al alloy. *Metals* **2020**, *10*, 594. [CrossRef]
4. Mandal, P.K.; Robi, P.S. Influence of micro-alloying with silver on microstructure and mechanical properties of Al-Cu alloy. *Mater. Sci. Eng. A* **2018**, *722*, 99–111. [CrossRef]
5. Li, B.; Pan, Q.; Huang, X.; Yin, Z. Microstructures and properties of Al–Zn–Mg–Mn alloy with trace amounts of Sc and Zr. *Mater. Sci. Eng. A* **2014**, *616*, 219–228. [CrossRef]
6. Huang, Y.; Zhang, C.; Ma, Y.; Liu, Y. Effects of homogenization on the dissolution and precipitation behaviors of intermetallic phase for a Zr and Er containing Al–Zn–Mg–Cu alloy. *Prog. Nat. Sci.* **2020**, *30*, 47–53. [CrossRef]
7. Freiberg, D.; Zhu, W.; Park, J.-S.; Almer, J.D.; Sanders, P. Precipitate characterization in model Al-Zn-Mg-(Cu) alloys using small-angle X-ray scattering. *Metals* **2020**, *10*, 959. [CrossRef]
8. Zhong, H.; Li, S.; Zhang, Z.; Li, D.; Deng, H.; Chen, J.; Qi, L.; Ojo, O.A. Precipitation behavior, mechanical properties, and corrosion resistance of rare earth–modified Al-Zn-Mg-Cu alloys. *Mater. Today Commun.* **2022**, *31*, 103732. [CrossRef]
9. Robson, J.; Prangnell, P.B. Dispersoid precipitation and process modelling in zirconium containing commercial aluminium alloys. *Acta Metall.* **2001**, *49*, 599–613. [CrossRef]
10. Nes, E. Precipitation of the metastable cubic Al3Zr-phase in subperitectic Al-Zr alloys. *Acta Metall.* **1972**, *20*, 499–506. [CrossRef]
11. Zhou, B.; Liu, B.; Zhang, S. The advancement of 7xxx series aluminum alloys for aircraft structures: A review. *Metals* **2021**, *11*, 718. [CrossRef]
12. Zuo, J.; Hou, L.; Shi, J.; Cui, H.; Zhuang, L.; Zhang, J. The mechanism of grain refinement and plasticity enhancement by an improved thermomechanical treatment of 7055 Al alloy. *Mater. Sci. Eng. A* **2017**, *702*, 42–52. [CrossRef]
13. Sun, Y.; Luo, Y.; Pan, Q.; Liu, B.; Long, L.; Wang, W.; Ye, J.; Huang, Z.; Xiang, S. Effect of Sc content on microstructure and properties of Al-Zn-Mg-Cu-Zr alloy. *Mater. Today Commun.* **2021**, *26*, 101899. [CrossRef]
14. Vo, N.Q.; Dunand, D.C.; Seidman, D.N. Improving aging and creep resistance in a dilute Al–Sc alloy by microalloying with Si, Zr and Er. *Acta Mater.* **2014**, *63*, 73–85. [CrossRef]
15. Guan, R.; Shen, Y.; Zhao, Z.; Wang, X. A high-strength, ductile Al-035.Sc-0.2 Zr alloy with good electrical conductivity strengthened by coherent nanosized-precipitates. *J. Mater. Sci. Technol.* **2017**, *33*, 215–223.
16. Liu, F.C.; Ma, Z.Y.; Zhang, F.C. High strain rate superplasticity in a micro-grained Al–Mg–Sc alloy with predominant high angle grain boundaries. *J. Mater. Sci. Technol.* **2012**, *28*, 1025–1030. [CrossRef]
17. Hyland, R.W. Homogeneous nucleation kinetics of Al3Sc in a dilute Al-Sc alloy. *Metall. Trans. A* **1992**, *23*, 1947–1955. [CrossRef]
18. Clouet, E.; Barbu, A.; Laé, L.; Martin, G. Precipitation kinetics of Al3Zr and Al3Sc in aluminum alloys modeled with cluster dynamics. *Acta Mater.* **2005**, *53*, 2313–2325. [CrossRef]
19. Riva, S.; Yusenko, K.V.; Lavery, N.P.; Jarvis, D.J.; Brown, S.G. The scandium effect in multicomponent alloys. *Int. Mater. Rev.* **2016**, *61*, 203–228. [CrossRef]
20. Sun, F.; Nash, G.L.; Li, Q.; Liu, E.; He, C.; Shi, C.; Zhao, N. Effect of Sc and Zr additions on microstructures and corrosion behavior of Al-Cu-Mg-Sc-Zr alloys. *J. Mater. Sci. Technol.* **2017**, *33*, 1015–1022. [CrossRef]
21. Chen, Y.; Gao, N.; Sha, G.; Ringer, S.P.; Starink, M.J. Microstructural evolution, strengthening and thermal stability of an ultrafine-grained Al–Cu–Mg alloy. *Acta Mater.* **2016**, *109*, 202–212. [CrossRef]
22. Tsivoulas, D.; Robson, J. Heterogeneous Zr solute segregation and Al3Zr dispersoid distributions in Al–Cu–Li alloys. *Acta Mater.* **2015**, *93*, 73–86. [CrossRef]
23. Zhao, H.; De Geuser, F.; da Silva, A.K.; Szczepaniak, A.; Gault, B.; Ponge, D.; Raabe, D. Segregation assisted grain boundary precipitation in a model Al-Zn-Mg-Cu alloy. *Acta Mater.* **2018**, *156*, 318–329. [CrossRef]
24. Qian, Y.; Xue, J.; Wang, Z.; Yang, Z.; Qian, P. Mechanical Properties Evaluation of Zr Addition in L12-Al3(Sc1−xZrx) Using First-Principles Calculation. *Jom* **2016**, *68*, 1293–1300. [CrossRef]
25. Spierings, A.B.; Dawson, K.; Heeling, T.; Uggowitzer, P.J.; Schäublin, R.; Palm, F.; Wegener, K. Microstructural features of Sc-and Zr-modified Al-Mg alloys processed by selective laser melting. *Mater. Des.* **2017**, *115*, 52–63. [CrossRef]
26. Röyset, J.; Ryum, N. Scandium in aluminium alloys. *Int. Mater. Rev.* **2005**, *50*, 19–44. [CrossRef]
27. Costa, S.; Puga, H.; Barbosa, J.; Pinto, A. The effect of Sc additions on the microstructure and age hardening behaviour of as cast Al–Sc alloys. *Mater. Des.* **2012**, *42*, 347–352. [CrossRef]
28. Tzeng, Y.-C.; Wu, C.-T.; Yang, C.-H.; Lee, S.-L. Effects of trace Be and Sc addition on the thermal stability of Al–7Si–0.6 Mg alloys. *Mater. Sci. Eng. A* **2014**, *614*, 54–61. [CrossRef]

29. Tzeng, Y.-C.; Nieh, J.-K.; Bor, H.-Y.; Lee, S.-L. Effect of trace Be and Sc additions on the mechanical properties of A357 alloys. *Metals* **2018**, *8*, 194. [CrossRef]
30. Mukhopadhyay, A.K.; Singh, V.; Prasad, K.S.; Chakravorty, C.R. On S (Al2CuMg) precipitation in an AlCuMg alloy containing small additions of beryllium. *Acta Mater.* **1996**, *44*, 3115–3124. [CrossRef]
31. Liu, X.; Zhang, P.; He, S.; Xu, Q.; Dou, Z.; Wang, H. Effect of beryllium content and heat treatment on microstructure and yield strength in Be/6061Al composites. *J. Alloys Compd.* **2018**, *743*, 746–755. [CrossRef]
32. Ogura, T.; Hirosawa, S.; Cerezo, A.; Sato, T. Atom probe tomography of nanoscale microstructures within precipitate free zones in Al–Zn–Mg (–Ag) alloys. *Acta Mater.* **2010**, *58*, 5714–5723. [CrossRef]
33. Won, S.-J.; So, H.; Kang, L.; Oh, S.J.; Kim, K.-H. Development of a high-strength Al-Zn-Mg-Cu-based alloy via multi-strengthening mechanisms. *Scr. Mater.* **2021**, *205*, 114216. [CrossRef]
34. So, H.; Won, S.-J.; Park, J.; Oh, S.J.; Kang, L.; Kim, K.-H. Mechanical properties and microstructural evolution in Al–Cu–Mg–Ag alloy with a CuxMgx/10 content. *Mater. Sci. Eng. A* **2021**, *824*, 141573. [CrossRef]
35. Park, M.-J.; So, H.; Kang, L.; Byeon, J.-W.; Kim, K.-H. The relation between mechanical properties and microstructural evolution induced by Sc microalloying in Al-20Zn-3Cu alloy. *J. Alloys Compd.* **2021**, *889*, 161719. [CrossRef]
36. Xiao, H.; Wang, Z.; Geng, J.; Zhang, C.; Li, Y.; Yang, Q.; Wang, M.; Chen, D.; Li, Z.; Wang, H. Precipitation and crystallographic relationships of nanosized η/η′precipitates at S-Al interface in Al-Zn-Mg-Cu alloy. *Scr. Mater.* **2022**, *214*, 114643. [CrossRef]
37. Zou, Y.; Wu, X.; Tang, S.; Zhu, Q.; Song, H.; Cao, L. Co-precipitation of T′ and η′ phase in Al-Zn-Mg-Cu alloys. *Mater. Charact.* **2020**, *169*, 110610. [CrossRef]
38. Mondal, C.; Mukhopadhyay, A.K. On the nature of T (Al2Mg3Zn3) and S (Al2CuMg) phases present in as-cast and annealed 7055 aluminum alloy. *Mater. Sci. Eng. A* **2005**, *391*, 367–376. [CrossRef]
39. Takata, N.; Ishihara, M.; Suzuki, A.; Kobashi, M. Microstructure and strength of a novel heat-resistant aluminum alloy strengthened by T-Al6Mg11Zn11 phase at elevated temperatures. *Mater. Sci. Eng. A* **2019**, *739*, 62–70. [CrossRef]
40. Knipling, K.E.; Karnesky, R.A.; Lee, C.P.; Dunand, D.C.; Seidman, D.N. Precipitation evolution in Al–0.1Sc, Al–0.1Zr and Al–0.1Sc–0.1Zr (at.%) alloys during isochronal aging. *Acta Mater.* **2010**, *58*, 5184–5195. [CrossRef]
41. Zhang, M.; Liu, T.; He, C.; Ding, J.; Liu, E.; Shi, C.; Li, J.; Zhao, N. Evolution of microstructure and properties of Al–Zn–Mg–Cu–Sc–Zr alloy during aging treatment. *J. Alloys Compd.* **2016**, *658*, 946–951. [CrossRef]
42. Karov, J.; Youdelis, W.; Herring, R. Clustering in Al–3Cu–0.1Be. *Mater. Sci. Technol.* **1986**, *2*, 547–551. [CrossRef]
43. Luo, A.; Youdelis, W.V. Microstructure and mechanical behavior of Al-Li-Cu-Mg alloy 8090 microalloyed with V and Be. *Metall. Trans. A* **1993**, *24*, 95–104. [CrossRef]
44. Youdelis, W.; Fang, W.; Lowes, T. Precipitation and age hardening behaviour of AI–0.2Ti–0.2Be alloy. *Mater. Sci. Technol.* **1990**, *6*, 1227–1230. [CrossRef]
45. Cao, Y.; Ni, S.; Liao, X.; Song, M.; Zhu, Y. Structural evolutions of metallic materials processed by severe plastic deformation. *Mater. Sci. Eng. R Rep.* **2018**, *133*, 1–59. [CrossRef]